Human-like Endtip Stiffness Modulation Towards Stable, Dexterous Manipulation

Anna Shafer and Ashish D. Deshpande

***Abstract*— The human hand is capable of successful, stable completion of amazingly complex and dexterous in-hand manipulation tasks through modulation of musculotendon stiffness. Although several studies have evaluated biomechanical stiffness for grasping and manipulation, no prior works have evaluated the effect of anatomical stiffness parameters on complex in-hand manipulation performance. In this work, we analyze the passive stiffness boundaries of a biomechanically accurate, tendon-driven human-like index finger to quantify the effect of stiffness parameter modulation on stability within the Cartesian workspace. The passive stiffness model shows that the greatest stiffness ellipsoid volume is aligned with efficient opposition of the anatomical thumb and bounds the conservatively stable region of the 3D workspace. Based on this model, we developed a biomechanically informed stiffness controller which increases the stable manipulation region and trajectory tracking performance within the reachable workspace. The result of this work is a method to quantify the stable manipulation region for tendon-driven systems that operate in a 3D space, enabling biomechanically informed mechanical and control design for stable, dexterous in-hand manipulation.**

I. Introduction

Humans have an inherent ability to modulate endtip stiffness to maintain stability and complete complex tasks with high levels of performance [1]. Achieving finger endtip stiffness control is challenging and rarely tackled by robotic hands, with one notable exception being the DLR Hand [2]. High endtip stiffness yields greater accuracy while lower endtip stiffness enables greater robustness to unexpected disturbances in the environment. Understanding the mechanisms of human stiffness modulation will enable robotic hands to improve stable, dexterous in-hand manipulation performance and better optimize for this trade-off of accuracy and robustness. Because of its critical contributions to fine hand function, index finger stiffness has been studied by both biomechanists and roboticists. Prior works have evaluated human index stiffness modulation through varying joint angles (pose) and co-contraction (coordinated stiffness of agonist and antagonist muscles) in a plane of actuation [3]. Pose is the best predictor of stiffness ellipse orientation and isotropy across subjects while co-contraction and active force generation have been correlated to intrasubject size of the ellipse [3], [4], [5]. Therefore, geometric patterns of endtip stiffness are not only predictable across subjects but potentially scalable based on muscular or grip strength, yet few studies have evaluated the varying endtip stiffness of the index finger in Cartesian space with the most comprehensive prior work in this area evaluating only the 2D workspace [4].

All authors are with the Department of Mechanical Engineering, The University of Texas at Austin, Austin, Texas 78712, USA ashish@austin.utexas.edu

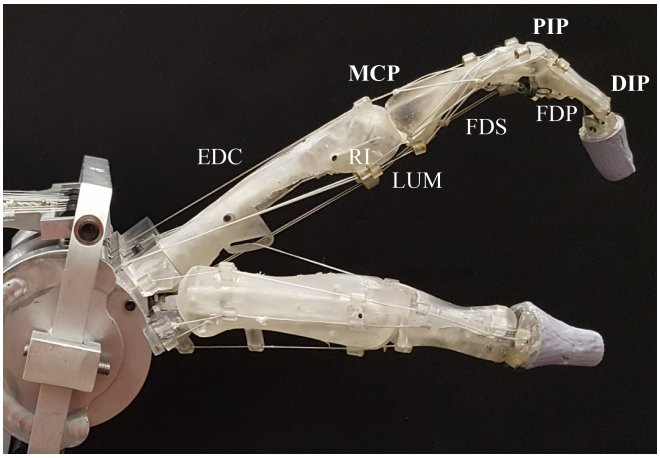

Fig. 1. The Anatomically Correct Testbed (ACT) Hand is designed as a physical simulation platform for understanding the underlying biomechanics of human hand motion [6]. Index finger muscle abbreviations: extensor digitorum communis (EDC), flexor digitorum superficialis (FDS), flexor digitorum profundus (FDP), lumbrical (LUM), radial interosseous (RI), and ulnar interosseous (UI). Joint angle abbreviations: metacarpophalangeal (MCP) abduction (ab)/adduction (ad), MCP flexion (flex)/extenstion (ext), peripheral interphalangeal (PIP) flex/ext, and distal interphalangeal (DIP) flex/ext.

The unique properties of the Anatomically Correct Testbed (ACT) hand, shown in Fig. 1, allow biomechanical principle observation in a repeatable setting while simultaneously allowing for the application of robotics tools for quantification and analysis of biomechanics. The mechanics of the hand have been validated against human cadaver data for anatomical accuracy of joint structure, range of motion, and actuator operated tendons mapped to anatomical muscles [6], [7], [8]. The anatomical accuracy of the ACT hand is not necessary for fine endtip force control; however, this capability is rare in existing robotic systems and the authors therefore believe that further insight can be gained from a human-like simulator.

Stable dexterity is required to successfully complete complex in-hand manipulation tasks where even slight vibrations in manipulator digits causes contact loss, resulting in grasp failure, or causes unrealizable configurations, resulting in task failure. Humans have an inherent ability to optimize finger stiffness to maintain grasp stability and complete complex task constraints with high levels of performance, yet the parameters for this optimization are not fully characterized [9]. Understanding the mechanisms of human stiffness modulation will enable robotic hands to improve stable,

dexterous manipulation capabilities and performance [1]. Passive stiffness analysis for tendon-driven robotics in 2D space has successfully predicted stable performance areas [10]. The human hand encounters forces in 3D space during dexterous manipulation; therefore, characterization of endtip stiffness should include all three anatomical planes.

The goal of this work is to demonstrate through modeling and experimental analysis on a human-like index finger, the effects of multi-joint finger endtip stiffness modulation on stable completion of dexterous manipulation tasks in the Cartesian workspace. This novel characterization of the effect of all degrees of freedom on the passive finger endtip stiffness is also the first work to evaluate conservative stability bounds of a tendon-driven endpoint in 3D Cartesian space. The result of this work is a generalizable method for tendon-driven robotic manipulators to optimize stiffness for greater accuracy without compromising robustness for the successful completion of complex tasks.

II. Biomechanical Stiffness Model

We developed a biomechanical model of index finger stiffness and validated this model using the human-like ACT hand. The stiffness of each tendon is measured by maintaining finger joint position and ramping tendon force up and down while recording tendon length and tension. Hooke's Law is then applied to find the spring constant for each tendon, which forms the diagonal muscle space stiffness matrix, K_m, seen in (1).

$$K_m = [K_{FDS}, K_{FDP}, K_{UI}, K_{EDC}, K_{RI}, K_{LUM}] \quad (1)$$

$$K_j = R(\boldsymbol{\theta}) K_m R^T(\boldsymbol{\theta}) \quad (2)$$

$$K_x = J^{-T}(\boldsymbol{\theta}) K_j J^{-1}(\boldsymbol{\theta}) \quad (3)$$

$$\boldsymbol{\theta} = \left[MCP_{ab/ad}, MCP_{flex}, PIP_{flex}, DIP_{flex}\right]^T \quad (4)$$

The moment arm matrix, $R(\boldsymbol{\theta})$, converts from muscle space, K_m, to joint space, K_j, where K_m is the series compliance of the system. Since the ACT hand has only one parallel compliance component, the ligament-like spring on the PIP joint which is not active during the functional manipulation workspace, only series compliance is used in this model [11]. Transformation to Cartesian space, K_x, is performed in (3), where $J(\boldsymbol{\theta})$ is the Jacobian matrix derived from serial chain kinematics of the Denavit-Hartenberg parameter model and (4) defines the joint angle vector, $\boldsymbol{\theta}$, with angles relative to the center of the previous phalange.

The four degrees of freedom (DOFs) of the index finger are controlled in four Cartesian DOFs, three translational ($\mathbf{x} \in \mathbb{R}^3$) and one rotational ($\phi_{dist} \in \mathbb{R}^1$). When performing Cartesian control, the underactuated PIP joint is not actively controlled; therefore, the first 3x3 of K_x corresponding to the three Cartesian axes is used for the passive analysis.

The passive endtip stiffness is visualized as an ellipse in Cartesian space by multiplying the stiffness matrix by small displacements in the shape of a circle [12]. Similarly, ellipses are calculated in each anatomical plane. The resulting anatomical stiffness ellipses from the model are shown for two poses, representative of the portion of the Sagittal plane

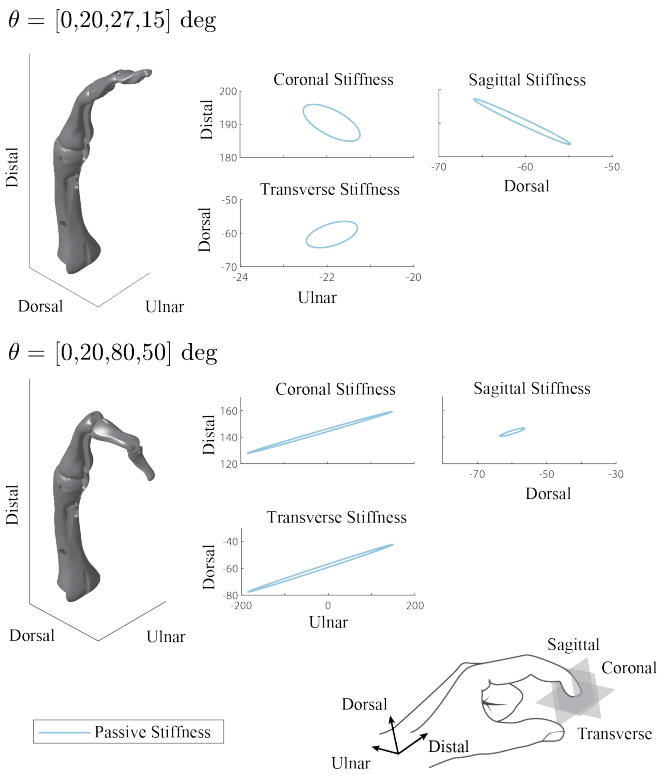

Fig. 2. Analyzing each anatomical plane shows variance within 3D space. Joint angles, $\boldsymbol{\theta}$, are defined as in (4). The extended position shows smaller stiffness in the Transverse and Coronal planes than the Sagittal plane while the flexed position shows orders of magnitude greater stiffness in the Transverse and Coronal planes.

where the ligaments are not active, in Fig. 2. The flexed pose is relatively compliant in the Sagittal plane but shows orders of magnitude more stiffness in the Transverse and Coronal planes. The extended pose demonstrates greater stiffness in the Sagittal plane and smaller stiffness in the Coronal and Transverse planes. This is due to the underlying anatomical structure which makes motion in the MCP abduction and adduction plane difficult when other joints are nearing their flexion limits.

The variance of the stiffness ellipsoid volume as it changes throughout the full, reachable workspace is shown in Fig. 3. The ellipsoid volume increases along the Dorsal axis, consistent with the increase in stiffness observed in the Transverse and Coronal planes. This highlights the naturally stiff regions of the index finger which are advantageous in precision tasks, particularly those involving the opposition of the thumb, such as writing.

The highest stiffness by volume is seen in the Palmar area of the workspace, caused by the greater stiffness magnitude along the Ulnar axis in the Distal region of the Sagittal plane. The implications for dexterous manipulation tasks are twofold. The areas of highest stiffness enable manipulation tasks involving pinch and precision grasps where the anatomical system can utilize the high stiffness to maintain precision. The areas of lower stiffness volume with higher Sagittal stiffness, seen at the edges of the workspace, prevent the finger from injury as it is compliant to disturbances while

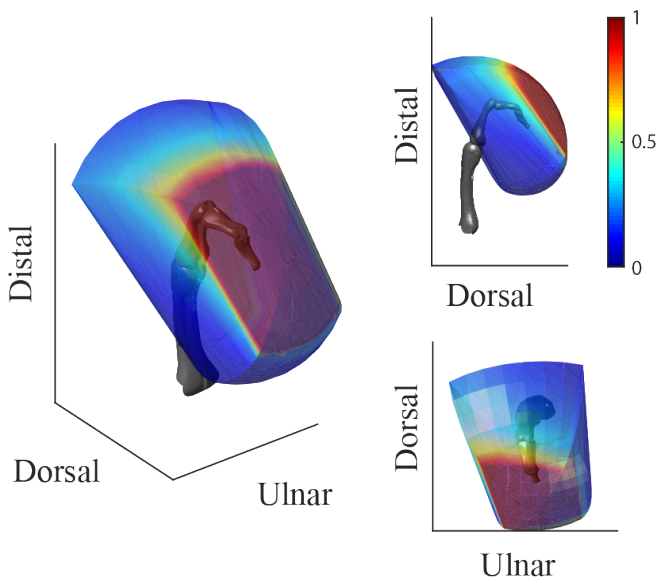

Fig. 3. Variance of the stiffness ellipsoid volume ($V = 4/3{*}\pi{*}\lambda_1{*}\lambda_2{*}\lambda_3$, where λ_n is the eigenvalue of K_x) throughout the 3D reachable workspace. Normalized and scaled to show variance with greatest stiffness at 1 and lowest at 0.

it is capable of less force production.

III. Stability Model

Passive stiffness analysis has been used to find stable areas within the workspace for tendon-driven robotic systems in two dimensions and the principle is scalable to other dimensions [10]. This conservative system passivity condition is applied at the desired level of control such as tendon, joint, or Cartesian space [13], [10]. In this work, we evaluate Cartesian space where the passive endtip stiffness, $K_{x,pass}$, must bound the desired active stiffness for the endtip, $K_{x,d}$, to satisfy the passivity bound for conservative stability (5).

$$K_{x,pass} - K_{x,d} > 0 \tag{5}$$

Quantifying the effect of stiffness on stable manipulation requires characterization of both passive and active stiffness parameters [14]. In this work, we use the conservative congruence transformation to transform from tendon (1) and joint space (6) to Cartesian space (7) to evaluate the passive stability bounds of the human-like ACT hand while accounting for internal muscle forces, $\mathbf{f_m}$, and external forces, $\mathbf{f_x}$, encountered during interactions with the environment.

$$K_j = R(\boldsymbol{\theta}) K_m R^T(\boldsymbol{\theta}) + \left[\frac{\partial R(\boldsymbol{\theta})}{\partial \boldsymbol{\theta}} \mathbf{f}_m\right] \tag{6}$$

$$K_x = J^{-T}(\boldsymbol{\theta}) K_j J^{-1}(\boldsymbol{\theta}) + \left[\frac{\partial J^T(\boldsymbol{\theta})}{\partial \boldsymbol{\theta}} \mathbf{f}_x\right] \tag{7}$$

$$\tag{8}$$

A. Model Definition

The stability of each point in the workspace is then evaluated for the conservative stability bound in (5) as a symmetric, positive definite test using the Cholesky factorization function in MATLAB (Mathworks, Inc). Mapping the

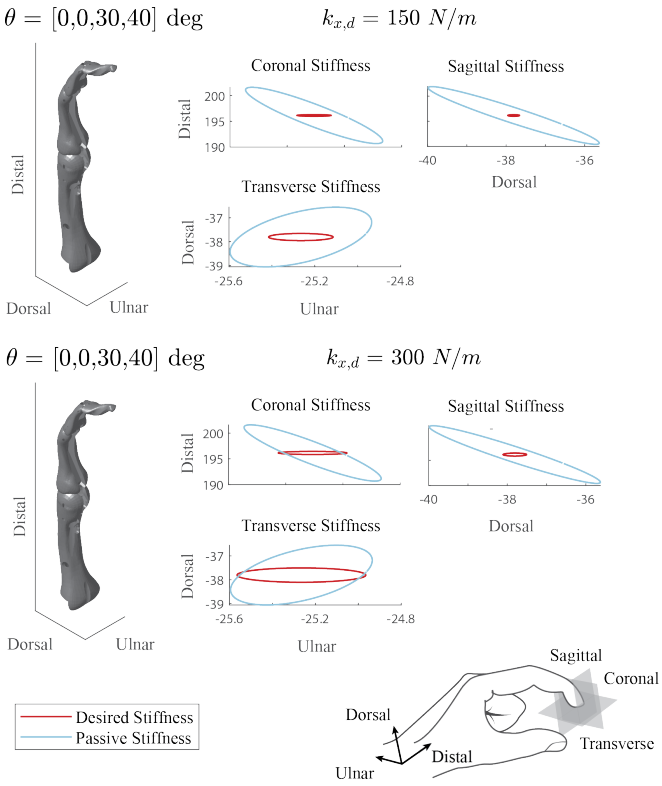

Fig. 4. Analyzing stability in each anatomical plane highlights which axes break the conservative stability criteria with isotropic desired stiffness. The system is stable initially with $k_{x,d} = 150\ N/m$, but the Transverse and Coronal planes violate stability bounds when desired stiffness doubles, $k_{x,d} = 300\ N/m$. The system remains bounded by passive stiffness in the Sagittal plane.

stability boundaries in the Cartesian space shows the effect of increased desired stiffness throughout the workspace as the passive stiffness changes due to geometry constraints as explored in II. The resulting stable workspace can then be analyzed on a task basis for robotic control design for manipulation.

Here, we utilize the passive stiffness model to characterize the effects of biomechanical geometric constraints on the stable region in 3D space. Fig. 4 illustrates the effect of desired stiffness parameters on stability and highlights the need to characterize stability criteria in each anatomical plane, since Cartesian points may appear stable in the Sagittal plane alone but fail the passivity criteria in other planes.

Setting the control gains to an isotropic value, $K_{x,d} = diag(k)$, highlights the areas of the workspace in which the passive stiffness of the system is highly anisotropic in shape and therefore breaks the conservative stability criteria as shown in Fig. 5. These areas are primarily along the edges of the workspace where the system approaches singularities and the anatomical system loses its mechanical advantage from tendons and begins to rely more on the stiffness of joint ligaments to prevent dislocations.

Isotropic gains are only required when high accuracy and therefore high stiffness is required in all directions. Unnecessarily high stiffness in any given direction leads to

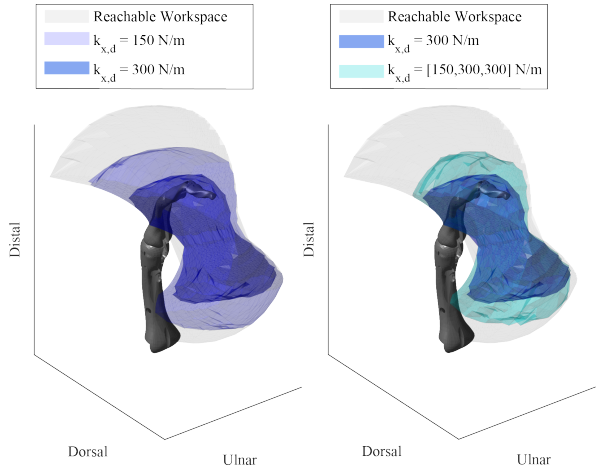

Fig. 5. Conservative stability boundaries within the reachable Cartesian workspace shown with isotropic desired stiffness. Doubling the desired stiffness decreases the stable region within the reachable workspace from 73% to 34%, (a). Stability boundaries with biomechanically informed controller stiffness, shown in Cyan, (b). Using geometric stiffness constraints to set $k_{ulnar} = 150\ N/m$ while $k_{distal} = k_{dorsal} = 300\ N/m$ yields an increased stable workspace volume of 54%.

inefficiency and potential loss of stability. Humans inherently modulate stiffness to maintain stability for manipulation task completion.

Analyzing geometric properties, we developed biomechanically informed control gains for dexterous manipulation. Applying this method on a task basis enables high trajectory tracking accuracy in a specific direction, without violating the passivity bounds of the system. To maintain the performance for a trajectory task in the Sagittal plane, the stiffness along the Ulnar axis was decreased based on the results of Fig. 4 and the resulting volume of the stable region increased by 20%, see Fig. 5(b).

This analysis shows that bounding the desired, active stiffness within the passive stiffness ellipsoid increases the stable region for dexterous manipulation. Further, the quantification of the stable region enables the optimization of the trade-off between accuracy and robustness, allowing for higher stiffness and therefore accuracy to be achieved for a given task without compromising the suitable manipulation region.

B. Trajectory Tracking

An extended pose of the index finger was evaluated in simulation and then experimentally with a step response using first isotropic desired stiffness, then biomechanically inspired control gains. Fig. 6(b) shows a stable step response with steady state error of 25%. The effect of doubling the desired isotropic stiffness is shown in Fig. 6(d) as the system quickly becomes unstable due to the high stiffness in the Transverse and Coronal planes which violate the passive stiffness bounds as seen in Fig. 4. The instability prevents successful completion of the step response task and would cause object drop in a manipulation task.

With biomechanically informed control gains, the stable workspace increased allowing for stable task completion with

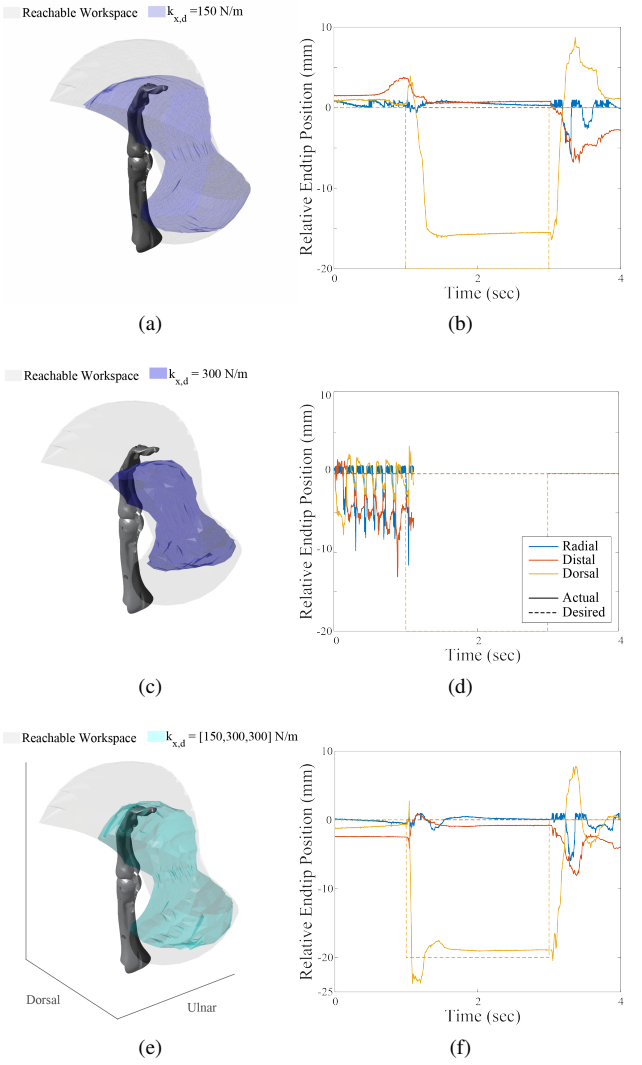

Fig. 6. Effect of stability boundary (left) when performing a step response within the workspace (right) for multiple stiffness control gains. A stable response to the commanded step with isotropic gains, $k_{x,d} = 150\ N/m$ (a), (b). Doubling the isotropic stiffness, $k_{x,d} = 300\ N/m$, caused an unstable response due to the high stiffness in the Transverse plane which violates the passivity bound (c), (d). Biomechanically inspired stiffness made a previously unstable area of the workspace stable for the higher desired stiffness in the Sagittal plane, allowing for better trajectory tracking performance (e), (f).

a higher desired stiffness and therefore greater accuracy, Fig. 6(f). This analysis shows the importance of evaluating passive stability bounds in 3D space to evaluate optimal areas of the workspace for task completion. Characterizing every controller, grasp, and force combination is beyond the scope of this work, but this method enables control design optimization of the accuracy and robustness trade-off for the successful completion of a given task.

C. Muscle Contributions

In biomechanical systems, changes in desired stiffness are accomplished by actively changing muscle activation patterns. Muscles are co-contracted to stiffen a particular joint or to coordinate complex motions with multi-articulate muscles. Prior work found finger endtip stiffnes modification

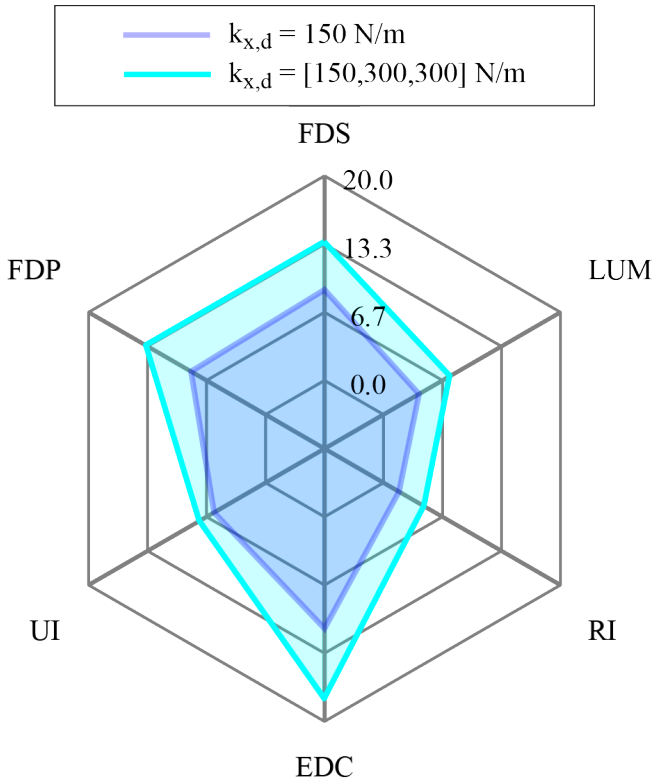

Fig. 7. Muscle forces recorded during step responses show co-contraction of the extensor and flexor muscles during the commanded step for initial stiffness $k_{x,d} = 150\ N/m$ and for biomechanically informed stiffness with increased desired stiffness in the task plane. At onset of the commanded trajectory, the co-contraction in the EDC, FDS, and FDP muscles nearly double as predicted.

while stationary to be linearly correlated with co-contraction of the EDC and FDS, but the study did not explicitly look at other muscle mappings and further work has not been done to fully characterize muscular contributions to stiffness [5]. The ACT hands human-like properties enable an analysis of the contributions of muscle groups to the modulation of stiffness in response to task or external stimulus.

The muscle contributions to the step responses in Fig. 6(a) and Fig. 6(c) were captured simultaneously with the position of the step response and are shown in Fig. 7.

The primary muscles used for the task in the Sagittal plane were the FDS, FDP, and EDC. These muscles co-contract to achieve greater stiffness at the endtip. Fig. 7 shows that the force application of these three muscles scaled linearly with the desired stiffness. This result aligned with prior work predicting a linear relationship between FDS and EDC activation and endtip stiffness [5]. Our study allowed the index finger to move while achieving the peak stiffness, which could explain the equal participation of the FDP muscle but further work is needed to fully characterize the relationship.

D. External Forces

Performing a dexterous in-hand manipulation task requires stable control of both the magnitude and orientation of the force application at the endtips [10]. The effect of changing magnitude and orientation on the stable workspace was characterized and examples of results are shown in Fig. 8 as a representation of the stiffness effect on the constant grasp force object manipulation task space.

The magnitude of the applied force had an inverse linear correlation ($R^2 = 0.92$) to the percent stable volume of the workspace. This finding was consistent with the prediction in prior work that the size of the ellipse would scale with the magnitude of the force [4].

The direction of the applied force had a large effect along the Ulnar axis. In the positive ulnar direction it caused an increase in the stable volume within the workspace, while a force applied in the negative ulnar direction decreased the stable region. This is significant given that many pinching tasks require forces along this axis due to the anatomical positioning of the thumb. By mapping the stable region with external forces similar to task requirements, the geometric stiffness shows that greater stiffness is aligned to advantageously oppose the anatomical thumb while maintaining stability.

The effect of the applied forces on the stable region was experimentally validated with isotropic and biomechanically inspired desired stiffness while disturbances were applied to the endtip. The greater degree of stiffness in the Transverse and Coronal planes in the flexed postures allowed the system to easily maintain the position, despite disturbances in these planes even at lower stiffness magnitudes. When the same desired stiffness was used at extended postures, error along the Ulnar axis quickly accumulated or the system violated the passivity bound and quickly went unstable. This illustrates the biomechanical advantage that a human-like index finger has in performing dexterous manipulation tasks inside the proximal workspace, such as precision and pinch grasps involving the thumb.

IV. Conclusions

By learning from human abilities to modulate stiffness, robotic hands can increase their stable, dexterous manipulation performance. In this work, we analyzed the underlying biomechanics of a human-like index finger and successfully predicted the passively stable areas within the 3D Cartesian workspace for successful trajectory tracking and robustness to external forces. Evaluating the effect of various stiffness parameters on the stable regions of the index finger enabled biomechanically inspired controller design which increased the performance of the system without compromising the stable region for manipulation.

Limitations of this model to evaluate biomechanical stiffness include a lack of reflexes and ligaments for joints other than the PIP in the testbed. Ligaments are known to contribute significantly to the overall stiffness of a joint; however, in anatomical systems, the primary purpose of ligaments is preventing dislocation or over-extension of joints. For example, the MCP joint ligaments have minimal effect in the 0° to 60° joint angle range which is the primary manipulation workspace [11]. In this work, both the MCP

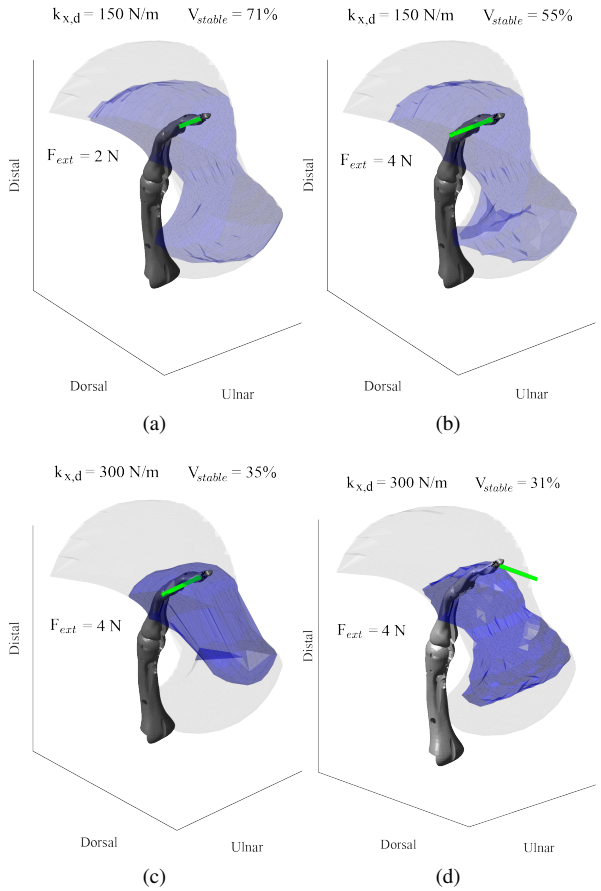

Fig. 8. Stability boundaries in the workspace shown with external force applied at a constant orientation to each point. Effect on stable region with increasing force magnitude (a) and (b) as the force applied along the Ulnar axis doubles from 2N to 4N and the stable region decreases by 24%. The isometric controller stiffness, $K_{x,d}$, is increased from 150 N/m (b) to 300 N/m (c) and constant external force applied in positive Ulnar direction. The direction of the force is varied in (d), showing a change in the shape of the stable region with a relatively stable volume.

and PIP joints are evaluated within their primary range and therefore experience minimal modelling effects from lack of ligaments. A future study could expand this model to evaluate the effect of ligaments on stability. Reflexes are also a component of dynamic stiffness in humans; however, this study is primarily concerned with the passive properties of the system, and therefore quantifying time-varying variables is outside the scope of this work.

A future work could also expand the analysis to additional phalanges and perform trajectory tasks with objects, while evaluating performance in the stable regions. The other fingers of the human hand would reasonably show similar stiffness properties, with some variation due to unique abduction and adduction muscle combinations. However, the thumb will have significantly different workspace results due to the underlying kinematic and muscular differences. The methods presented here are suitable for evaluating the stiffness properties for any tendon-driven phalange, anatomical or robotic, and can lend insight into stable stiffness controller design for endtip manipulation.

This predictive model of the passive stiffness of a complex multi-DOF tendon-driven system enables the evaluation of task constraints for optimal grasp synthesis or optimization of the stable workspace of the system given task parameters such as grasp force. This work also enables the mechanical and control design of future multi-DOF hands for increased dexterous manipulation performance in 3D space.

REFERENCES

[1] J. M. Inouye and F. J. Valero-Cuevas, "Muscle Synergies Heavily Influence the Neural Control of Arm Endpoint Stiffness and Energy Consumption," *PLOS Computational Biology*, 2016.

[2] M. Grebenstein, M. Chalon, W. Friedl, S. Haddadin, T. Wimböck, G. Hirzinger, and R. Siegwart, "The hand of the DLR hand arm system: Designed for interaction," *The International Journal of Robotics Research*, vol. 31, no. 13, pp. 1531–1555, 2012.

[3] A. Z. Hajian and R. D. Howe, "Identification of the Mechanical Impedance at the Human Finger Tip," *Journal of Biomechanical Engineering*, vol. 119, pp. 109–114, 1997.

[4] T. Milner and D. Franklin, "Characterization of multijoint finger stiffness: dependence on finger posture and force direction," *IEEE Transactions on Biomedical Engineering*, vol. 45, no. 11, pp. 1363–1375, 1998.

[5] M. Rossi, A. Altobelli, S. B. Godfrey, A. Ajoudani, and A. Bicchi, "Electromyographic mapping of finger stiffness in tripod grasp: A proof of concept," in *IEEE International Conference on Rehabilitation Robotics*. IEEE Computer Society, Sep 2015, pp. 181–186.

[6] A. D. Deshpande, Z. Xu, M. J. V. Weghe, B. H. Brown, J. Ko, L. Y. Chang, S. M. Wilkinson, David D .and Bidic, and Y. Matsuoka, "Mechanisms of the Anatomically Correct Testbed Hand," *IEEE/ASME Transactions on Mechatronics*, vol. 18, no. 1, pp. 238–250, 2013.

[7] T. D. Niehues and A. D. Deshpande, "Variable Thumb Moment Arm Modeling and Thumb-Tip Force Production of a Human-Like Robotic Hand," *Journal of Biomechanical Engineering*, vol. 139, 2017.

[8] ——, "Human-inspired object manipulation control with the anatomically correct testbed hand," in *IEEE International Conference on Robotics and Automation (ICRA)*, 2018, pp. 6861–6866.

[9] V. R. Garate, M. Pozzi, D. Prattichizzo, N. Tsagarakis, and A. Ajoudani, "Grasp Stiffness Control in Robotic Hands Through Coordinated Optimization of Pose and Joint Stiffness," *IEEE Robotics and Automation Letters*, vol. 3, no. 4, pp. 3952–3959, Oct 2018.

[10] P. Rao and A. D. Deshpande, "Analyzing and Improving Cartesian Stiffness Control Stability of Series Elastic Tendon-Driven Robotic Hands," in *IEEE International Conference on Robotics and Automation (ICRA)*, 2018.

[11] P.-H. Kuo and A. D. Deshpande, "Muscle-tendon units provide limited contributions to the passive stiffness of the index finger metacarpophalangeal joint," *Journal of Biomechanics*, vol. 45, no. 15, pp. 2531–2538, Oct 2012.

[12] R. Shadmehr, F. A. Mussa-Ivaldi, and E. Bizzi, "Postural Force Fields of the Human Arm and Their Role in Generating Multijoint Movements," *The Journal of Neuroscience*, vol. 13, no. l, pp. 45–62, 1993.

[13] P. Rao, G. C. Thomas, L. Sentis, and A. D. Deshpande, "Analyzing Achievable Stiffness Control Bounds of Robotic Hands with Compliantly Coupled Finger Joints," in *EEE International Conference on Robotics and Automation (ICRA)*, 2017.

[14] S.-F. Chen and I. Kao, "Conservative Congruence Transformation for Joint and Cartesian Stiffness Matrices of Robotic Hands and Fingers," *The International Journal of Robotics Research*, vol. 19, no. 9, pp. 835–847, Sep 2000.